Remarkably enhanced photoluminescence of hexagonal $GdPO_4 \cdot nH_2O$:Eu with decreasing size

2010 Nanotechnology 21 365709

(http://iopscience.iop.org/0957-4484/21/36/365709)

Nanotechnology **21** (2010) 365709 (7pp) doi:10.1088/0957-4484/21/36/365709

Remarkably enhanced photoluminescence of hexagonal $GdPO_4 \cdot nH_2O$:Eu with decreasing size

Shaozhe Lu[1], **Jiahua Zhang, Jishen Zhang, Haifeng Zhao, Yongshi Luo and Xinguang Ren**

Key Laboratory of Excited State Processes, Changchun Institute of Optics, Fine Mechanics and Physics, Chinese Academy of Sciences, 16 Eastern South Lake Road, Changchun 130033, People's Republic of China

E-mail: lusz@ciomp.ac.cn

Received 20 June 2010, in final form 28 July 2010
Published 13 August 2010
Online at stacks.iop.org/Nano/21/365709

Abstract

The hexagonal rhabdophane-type $GdPO_4$ hydrate ($GdPO_4 \cdot nH_2O$) was synthesized via a simple hydrothermal process. The size and morphology of the products can be tunable by adjusting the pH of reaction systems through the addition of aqueous NaOH. The nanorods with a width of 50–100 nm and a length of about 1 μm were obtained in the absence of NaOH (pH = 2), while a significant reduction of size (width: ~10 nm, length: ~50 nm) was observed for the product synthesized in the presence of NaOH (pH = 10). Surprisingly, the small-sized product exhibits a remarkably enhanced photoluminescence quantum yield and long excited state lifetime in comparison with those of the large-sized product. This abnormal luminescence phenomenon is discussed and explained. The EDS and XPS measurements revealed the presence of Na^+ in the small-sized samples. These Na^+ cations were probably bonded to the surface O^{2-} dangling bonds, which thus reduces the number of surface defects that usually serve as the nonradiative energy transfer center channels. A considerable reduction of surface defect centers results in the increase of the emission efficiency and excited state lifetime in a small-sized sample. Obviously, the controlled synthesis of rare-earth-doped nanoparticles with a small size, but with relatively strong luminescence, is significant for their applications in the areas of technologies including optoelectronics, sensing and bioimaging.

(Some figures in this article are in colour only in the electronic version)

1. Introduction

With the advances in display technology, the demand to increase the display resolution is becoming urgent. The use of nanosized luminescence materials may be an effective way to realize this demand. A number of papers reported previously demonstrated that the luminescent nanomaterials exhibit a significant size effect, surface effect and macroscopic quantum tunneling effect, and hence produce several unusual photophysical properties, compared with the corresponding bulk materials [1–3]. But, these size- and surface-induced effects also significantly modify the luminescence dynamics properties including the light absorption, excited state lifetime, energy transfer and so on. It is often found that the nanosized luminescent materials with smaller particle sizes have lower luminescence quantum yields and shorter fluorescence lifetimes than those of materials with larger particle sizes or the corresponding bulk materials [4, 5]. These weaknesses mainly originated from the complicated surface states such as the disordered environments around surface atoms [6], the existence of uncoordinated dangling bonds [7, 8] and a number of surface adsorptions [9, 10], which commonly act as nonradiative relaxation channels to decrease the luminescence quantum yield.

But a few unexpected luminescence phenomena were also observed by several research groups. Tissue's group [11] believed that the broadening of spectral lines, as well the increase of the Eu^{3+} $^5D_0$ lifetime, should be attributed to

[1] Author to whom any correspondence should be addressed.

the decrease of the particle size. Bhargava's group [12] reported that the decrease of particle size could increase the luminescence efficiency of Y_2O_3:Tb. Wakefield *et al* [13] reported that the Y_2O_3:Eu^{3+} nanomaterials had higher emission quantum efficiency than that of the corresponding bulk materials upon cathode-ray excitation. Obviously, it is necessary to enhance the luminescence efficiency of nanomaterials for their potential applications in the optoelectronics, biological and medical fields. Therefore, considerable efforts have been made to design some strategies, such as the novel synthetic route [14–16], energy transfer [17, 18], doping [19, 20], structure transformation [21] and surface treatments [22–24], for improving the luminescent efficiency. Di *et al* [18] reported that the $TbPO_4$ nanocrystals doped with a tiny amount of Eu^{3+} show a twofold increase of luminescence quantum yield, compared with the undoped $TbPO_4$, due to an efficient Tb^{3+}-to-Eu^{3+} energy transfer. Jia *et al* [21] synthesized $LaVO_4$:Eu nanocrystals of metastable zircon type at a low temperature using an ethylenediamine tetraacetic acid (EDTA)-assisted hydrothermal method. They found that the emission intensity of synthesized $LaVO_4$:Eu with zircon structure is nine times higher as that of $LaVO_4$:Eu with monazite structure that is prepared via the high-temperature solid-state reaction.

Rare earth orthophosphates ($RePO_4$) represent an important family of materials, and they have been used as active components in a wide range of applications such as high performance luminescent devices, magnets, catalysts, time-resolved fluorescence labels for biological detection and other functional materials based on the electronic, optical and chemical characteristics resulting from the 4f shell of their ions [17, 25, 26]. Very recently, the research interest regarding $RePO_4$ has been focused mainly on new synthetic methods and their novel potential in applications. Feldmann and co-workers [14] synthesized luminescent $LaPO_4$:Ce, Tb nanoparticles with a high quantum yield using a microwave-assisted synthesis method with ionic liquids as the reaction media. Luo *et al* [27] reported the synthesis of the cubic ordered mesoporous yttrium phosphate (YPO_4) via a hard template method and their photoluminescence properties. Di *et al* [28] reports for the first time on a new finding of luminescent $CePO_4$:Tb nanocrystals providing a novel oxygen sensing material on the basis of the redox responsive reversible luminescence in an oxidizing/reducing atmosphere. Zhang *et al* [29] used a simple and effective template-mediated protocol to synthesize $CePO_4$:Tb nanowires and demonstrated their potential applications in biological imaging and cellular labeling.

In this work, we investigated the relationship between the size and the photoluminescence properties of $GdPO_4$:Eu on the basis of the size-controlled synthesis of nanomaterials by adjusting the pH of reaction systems. Interestingly, an abnormal phenomenon, that the small-sized sample exhibits remarkably enhanced photoluminescence efficiency in comparison with that of the large-sized sample, was observed. The possible reasons were discussed based on the EDS, XPS and luminescence lifetime analyses. Our present results indicate that the luminescent rare-earth-doped nanomaterials are promising for their applications in the technological areas of nano-optoelectronics, biosensing and bioimaging, since a small size, but markedly enhanced emission efficiency for nanoscaled materials can be achieved by the controlled synthesis.

2. Experimental section

2.1. Synthesis

Rare earth nitrate ($Gd(NO_3)_3$ and $Eu(NO_3)_3$) stock solutions of 0.05 M were prepared by dissolving the corresponding metal oxide in concentrated HNO_3 at elevated temperatures. In a typical procedure using NaOH to adjust pH, 1 mmol of $(NH_4)_2HPO_4$ were dissolved in 15 ml of deionized water. 20 ml of $Gd(NO_3)_3$ and $Eu(NO_3)_3$ mixed solutions of 0.05 M (Gd:Eu = 19:1) was added to the above solution. The pH of the resulting solution was adjusted to 10 by the addition of an appropriate amount of aqueous NaOH. The solutions were then stirred at room temperature for 1 h. After that, the reaction mixtures were transferred into a 60 ml Teflon-lined autoclave. The autoclave was sealed and maintained for 12 h at 180 °C. After cooling down the autoclave to room temperature, the precipitation was separated by centrifugation, washed with deionized water and ethanol several times, and finally dried overnight under air at 60 °C. For the sample synthesized in the absence of NaOH, the synthetic procedure was the same, except that the pH of the resulting reaction solution was adjusted to 2. For 3%-Eu-doped samples, the synthetic procedure was the same except for the amount of Eu^{3+}.

2.2. Measurements

X-ray powder diffraction (XRD) data were collected on a Siemens D5005 diffractometer with Cu Kα radiation (λ = 1.5418 Å). The transmission electron microscope (TEM) images and high resolution transmission electron microscope (HRTEM) images of the samples were taken by a 200 kV field emission transmission electron microscope (TECNAI F20). Thermogravimetric analysis (TGA) was carried out on a Perkin-Elmer DTA 1700 differential thermal analyzer. The energy dispersive spectroscopy (EDS) was carried out on an energy dispersive spectrograph (Hitachi S-4800, GENESIS2000XMS60S). The x-ray photoelectron spectrum (XPS) was measured with the ESCALAB 250 x-ray photoelectron spectrograph. The emission and excitation spectra were measured with a Hitachi F-4500 spectrophotometer equipped with a continuous 150 W Xe arc lamp. The powder samples were fixed on a Cu sample holder during measuring and the measuring conditions were the same for all samples. In lifetime measurements, the fourth (266 nm) harmonic of an Nd:YAG laser (Spectra-Physics, DCR130) was used as an excitation source which had a linewidth of 0.2 cm^{-1}, pulse duration of 10 ns and repetition frequency of 10 Hz. The signals were detected with an oscilloscope model (TDS 3052). The luminescence quantum yield was measured on a Fluorescence SENS–9000 PL calibrated spectrometer equipped with an integrated sphere. For comparison of

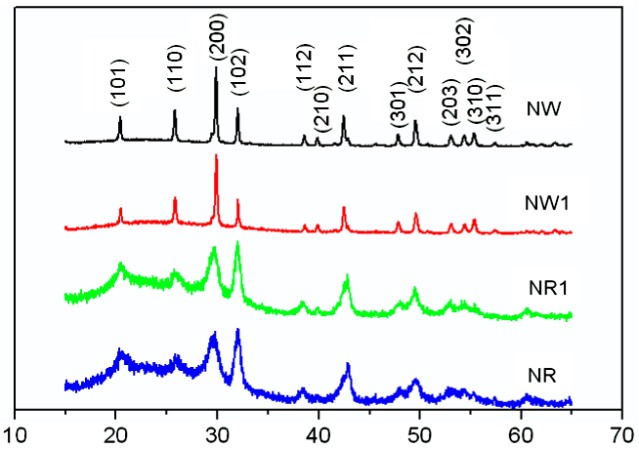

Figure 1. XRD patterns of samples NR (5%-Eu, pH = 10), NR1 (3%-Eu, pH = 10), NW (5%-Eu, pH = 2) and NW1 (3%-Eu, pH = 2).

different samples, the measurements were carried out at a fixed bandpass with the same instrument parameters.

3. Results and discussion

3.1. Size, morphology and composition analysis

The structure and crystallinity of the products were studied by XRD. Figure 1 shows the XRD patterns of the as-synthesized samples for different synthetic conditions. For simplicity, the 3% Eu-doped samples synthesized in the presence and absence of NaOH were labeled as NR1 and NW1, and the 5% Eu-doped samples as NR and NW, respectively, in all the descriptions. All the as-synthesized samples are crystalline and show diffraction peaks that can be well indexed to the hexagonal rhabdophane-type $GdPO_4$ hydrate ($GdPO_4{\cdot}nH_2O$) phase (JCPDS card no. 39-0232). No additional diffractions that could be attributed to impurities are observed. It is worth noting that a significant difference can be clearly observed for the width and relative intensity of the diffraction peaks of samples synthesized at different pH conditions. The samples synthesized in the presence of NaOH (pH = 10) exhibit markedly broad diffraction peaks and relatively weak diffraction of the (200) peak in contrast with those of the samples synthesized without any addition of NaOH (pH = 2), indicating a smaller size and possibly changed morphologies for the sample synthesized in the conditions with the addition of NaOH. This is further demonstrated by TEM observations below.

The size and morphology of the samples were characterized by TEM. Figures 2(a) and (b) present the TEM images of samples synthesized in the presence and absence of NaOH, respectively. It is observed clearly that the particle size is markedly different. The sample synthesized in the absence of NaOH (pH = 2) is composed of nanorods with an average width of 50–100 nm and an average length of about 1 μm; but for the sample synthesized in the presence of NaOH (pH = 10), a significantly decreased size and aspect ratio were observed (width: ∼10 nm; length: ∼50 nm). The difference in the size and morphology should be ascribed to the difference in the pH of the reaction. The pH of the reaction solution usually affects the crystal structure and morphology of the products in very complicated ways, as observed in the synthesis of many inorganic compounds [30–33]. However, the exact mechanism of the pH effect is not clear to date. Some possible explanations are given here. First, the variation of pH can significantly affect the reaction equilibrium and reaction ratio, which is able to tune the growth speed and control the size of crystals [34]. Second, pH can modify the relative growth ratio of the crystallographic facets, leading to the variation of crystal growth habit [35]. As observed in TEM images, the nanorods synthesized at pH 10 show a remarkably reduced aspect ratio compared with those synthesized at pH 2. Finally, the impurity adsorption (Na^+) at the surface might effectively inhibit the crystal growth [36], leading to the reduced size for the samples synthesized in the presence of NaOH.

A deeper insight into the crystalline quality, preferential growth axis and the exposed facets of the particles is obtained from HRTEM studies. Figures 2(c) and (d) show HRTEM micrographs recorded from samples synthesized in the presence and absence of NaOH, respectively. All observed particles are single crystalline, revealing lattice fringes that are in agreement with the corresponding lattice planes of the $GdPO_4$ hydrate phase that was also found by XRD. In the presence and absence of NaOH, the growth of the particles proceeds mainly along the *c* axis ⟨001⟩, leading to the observed rod-shaped particles, which is in agreement with the result observed for the hexagonal rhabdophane-type $TbPO_4$ hydrate that also exhibited a rod-like shape due to the preferential growth along the *c* axis [7, 18]. The precursor solution pH and the introduction of alkali metal cations (discussed below) might be the dominant effects to modify the particle sizes and morphologies of the products.

A typical TGA plot of as-synthesized $GdPO_4{\cdot}nH_2O$ was given in figure 3. Two weight losses occur in two distinct steps with an overall weight loss of 4.5% from 40 to 400 °C. The first one occurs in the temperature range 30–120 °C, and is assigned to the release of residual water adsorbed at the powder surface due to the storage in air condition. The second weight loss (4%) begins at about 120 °C; this corresponds to the dehydration of the hydrated hexagonal $GdPO_4$ [7]. The weight loss of 4% resulting from the dehydration corresponds to about 0.7 mol H_2O in the $GdPO_4{\cdot}nH_2O$ (n = ∼0.7).

3.2. Photoluminescence properties

Figure 4 (left) shows the room temperature excitation spectra of all the samples monitored within the $^5D_0 \rightarrow {}^7F_1$ transition of Eu^{3+}. A broad band with a maximum at 240–250 nm originates from the excitation of the oxygen-to-europium charge transfer band (CTB). The general f–f transitions within the Eu^{3+} $4f^6$ electron configuration in the longer wavelength region (280–340 nm) can also be observed. These peaks correspond to the direct excitation of the Eu^{3+} ground state into higher levels of the 4f manifold [37]. The observation of the Gd^{3+} $^8S_{7/2} \rightarrow {}^6I_J$ transition located at 274 nm suggests the existence of a Gd^{3+}-to-Eu^{3+} energy transfer.

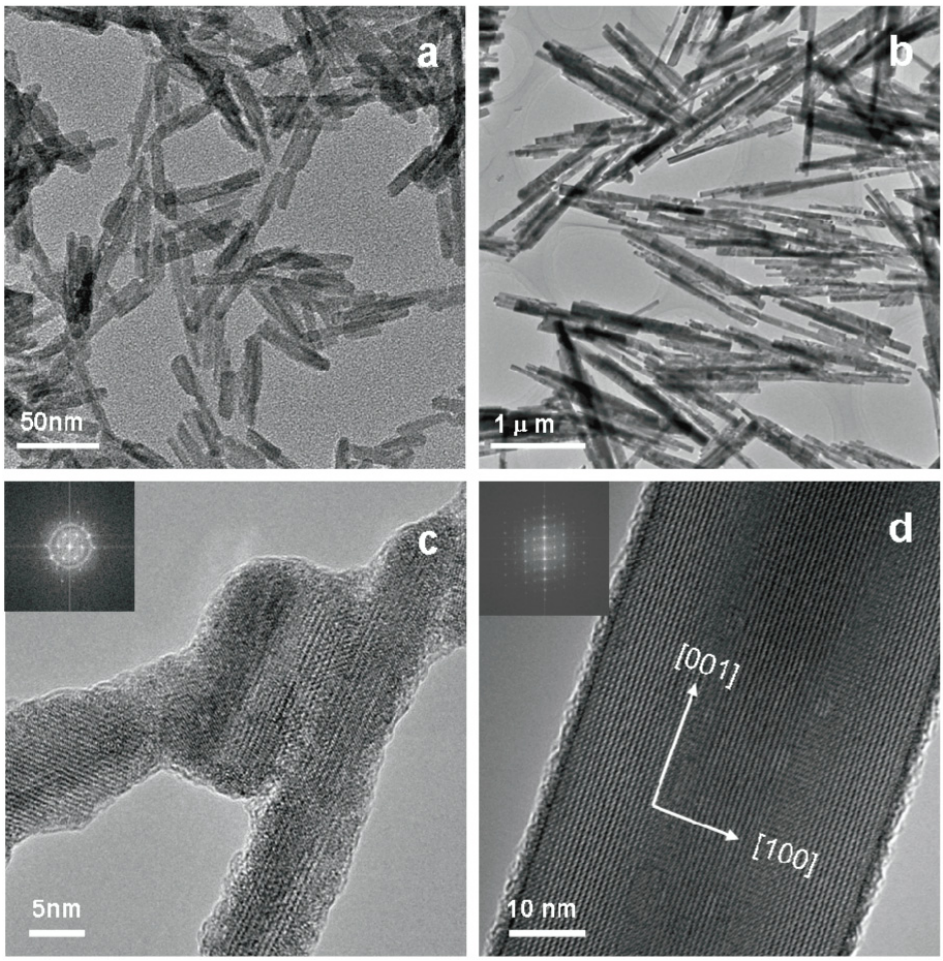

Figure 2. TEM images recorded from as-synthesized samples: (a) and (c) NR; (b) and (d) NW. The insets are the fast Fourier transform diffraction patterns (FFT).

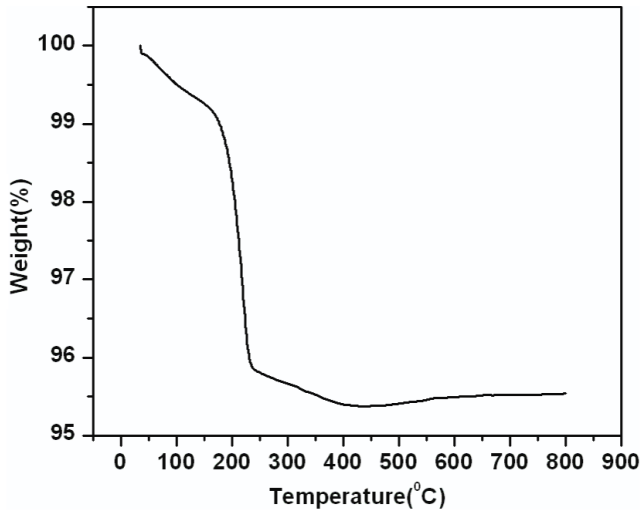

Figure 3. TGA curve of sample NR.

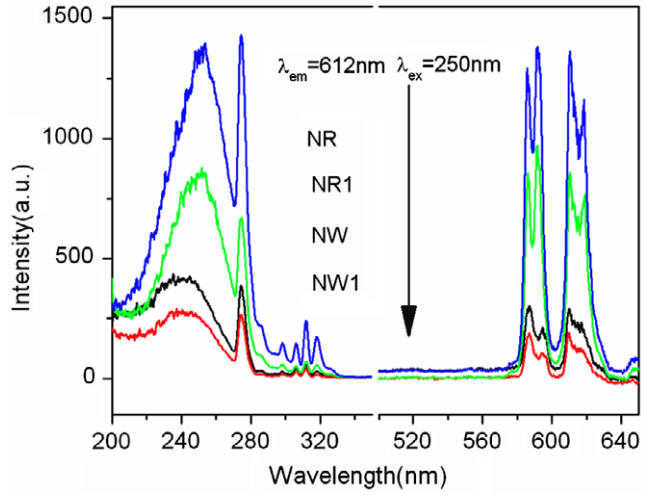

Figure 4. The excitation spectra (left) of $GdPO_4:Eu^{3+}$ samples measured at room temperature and monitored at 612 nm (left). The emission spectra (right) of the samples measured at room temperature and excited at a maximum of the CTB band.

It is worth noting that the CTBs of NR and NR1 are obviously 10 nm redshifted in contrast to those of NW and NW1. More surprisingly, the intensities of all the excitation peaks for samples NR and NR1 with a small size are much higher than those of the corresponding NW and NW1 with significantly increased size, respectively. This implies that the emission efficiency of samples NR and NR1 with a small size should be much higher than that of the corresponding NW

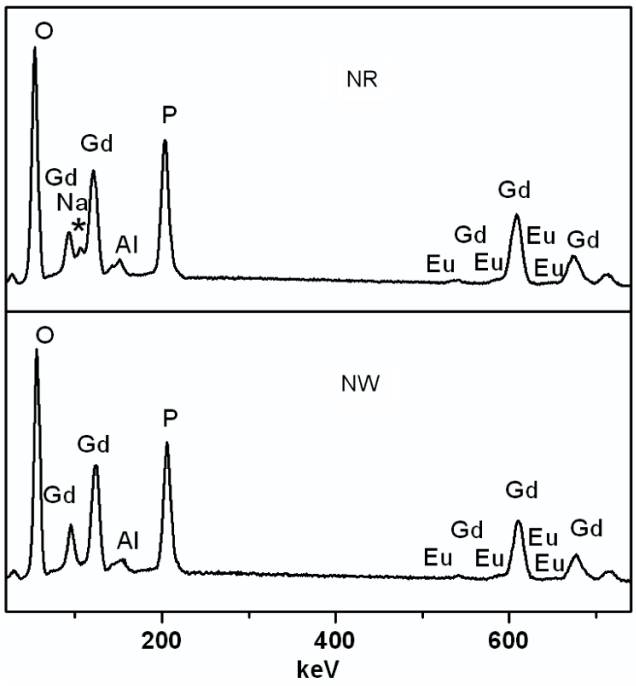

Figure 5. EDS spectra of samples NR and NW.

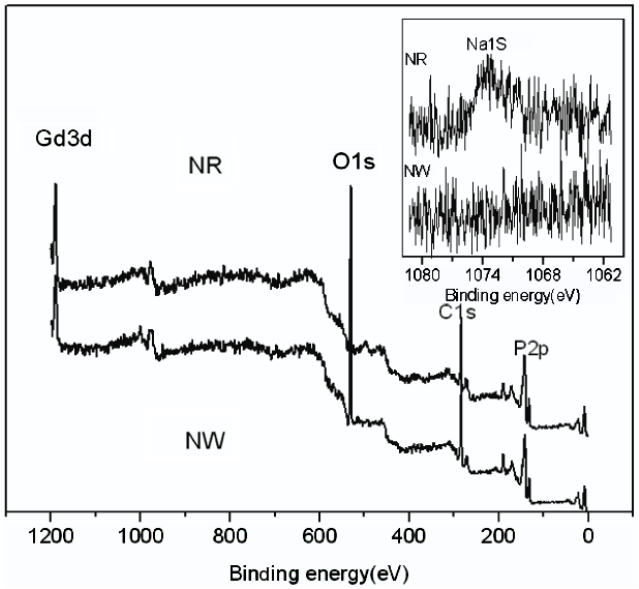

Figure 6. XPS spectra of samples NR and NW.

and NW1 at the same excitation conditions. Figure 4 (right) displays the emission spectra of all samples upon excitation of a CTB. The spectral peaks located in the range 580–660 nm originate from the Eu^{3+} $^5D_0 \rightarrow {}^7F_1$ and $^5D_0 \rightarrow {}^7F_2$ transitions. It can be seen that the emission intensity of the 5% Eu-doped sample is higher than that of the 3% Eu-doped sample synthesized at the same conditions. This is attributed to a high dopant concentration. As discussed above, for the samples doped with the same Eu^{3+} concentration, but synthesized at different conditions, a significant difference in the emission intensity is clearly observed. The integrated luminescence intensity of samples NR and NR1 is nearly four times stronger than that of the corresponding NW and NW1, respectively, that is, the luminescence of the sample with a small size is much higher than that of the sample with a remarkably increasing size at a given dopant concentration. This unusual phenomenon obviously contradicts the general results. Generally, the small-sized materials emit relatively weak luminescence in comparison with the large-sized materials due to a low crystallinity and the presence of a large number of surface defects such as the disordered environments around the surface atoms and uncoordinated dangling bonds, which commonly act as nonradiative relaxation channels to decrease the luminescence quantum yield.

To gain an insight into this abnormal phenomenon, we consider whether the addition of NaOH is a leading factor in strongly affecting the photoluminescence properties, since the difference in as-synthesized samples lies only in the pH variation of reaction systems arising from the addition of NaOH. Therefore, the energy dispersive spectrograph (EDS) and x-ray photoelectron spectrum (XPS) measurements were conducted to compare the difference of samples NR and NW.

Figure 5 shows the EDS spectrum of samples NR and NW, respectively. Both samples consist of Gd, Eu, P and O. The presence of the Al peak is due to the aluminum used as the sample holder in the measurements. It is worth noting that the element Na was detected for sample NR synthesized in the presence of NaOH. Similar to the EDS observation, the XPS spectrum (figure 6) further revealed the presence of Na^+ in sample NR since the characteristic peak of Na 1s was observed in the range 1060–1082 eV for sample NR (the inset of figure 6). The Gd(Gd 3d), P(P 2p) and O(O 1s) elements were observed for both samples. The EDS and XPS results confirm the presence of Na^+ in sample NR, indicating that the Na^+ cations from NaOH as a pH modifier are likely to introduce into the host lattice. Meanwhile, it is found that the content of Na^+ obtained by the calculation from XPS (1.37%) is lower that obtained by the calculation from EDS (2.7%). This difference is attributed mainly to the difference in detection depth using EDS and XPS. As we know, XPS measurements are based on the material's surface within a scale of about 3 nm. From the difference of Na^+ content from EDS and XPS measurements, we can conclude that the distribution of Na^+ is located not only at the surface of particles, but also in the interior of nanocrystals.

Mooney [38] and Su [39] have pointed out that, for $LnPO_4$ (Ln = La–Nd) with hexagonal crystal structure, there were oxygen chains, leaving some linear open tunnels along the *c* axis. The tunnels could be filled partly by water molecules and the filling did not change the crystal structure. Mooney [38] also pointed out that several metal cations could also be allowed to enter the tunnels. Therefore, we think that some Na^+ cations are likely to enter these open tunnels. In addition, at the surface of $GdPO_4$:Eu nanorods, there should exist a number of O^{2-} dangling bonds. Some Na^+ cations were probably bonded to the O^{2-} dangling bonds to stabilize the surface of particles. Except for the XPS observation that demonstrated the presence of Na^+ at the surface, we also

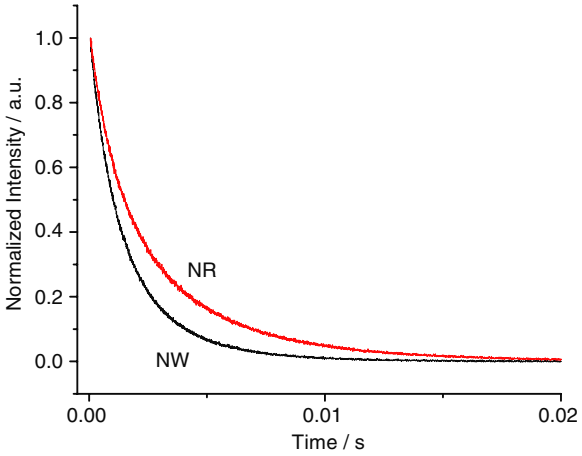

Figure 7. The fluorescence lifetime curves of NR and NW monitored at 612 nm emission of Eu^{3+}.

have additional reasons to prove this result. On the one hand, as discussed above in the excitation spectra, the CTBs of samples NR and NR1 are obviously 10 nm redshifted in contrast to those of NW and NW1. The position of CTB is related to the length of the Eu–O bond: the longer the Eu–O bond is, the longer the wavelength of the CTB position will be [1, 40]. Therefore, it can be deduced that the average distance of the Eu–O bond in the small-sized sample NR is longer than that in the large-sized NW. The lengthening of the Eu–O bond distance in sample NR is attributed to the fact that the radius of Na^+ (0.102 nm) is larger than that of Gd^{3+} (0.093 nm) and Eu^{3+} (0.094 nm). The bonding of Na^+ to O^{2-} increases the average distance of the metal–oxygen bond. On the other hand, the surface defects of nanomaterials such as the dangling bonds commonly serve as the serious luminescence quenching channels. Therefore, the presence of surface defect decreases the emission efficiency and the excited state lifetime of luminescence centers significantly. The bonding of Na^+ with the surface O^{2-} dangling bonds reduces the number of surface defects. The comparison of the lifetime of the Eu^{3+} $^5D_0$ state for samples NW and NR confirmed this result. It can be seen from figure 7 that the lifetime of Eu^{3+} $^5D_0$ of sample NR (2.86 ms) is relatively long in comparison with that of sample NW (1.67 ms), indicating a significant reduction of the surface defects in sample NR in comparison with that in sample NW. Therefore, a considerable reduction of surface defect centers due to the bonding of Na^+ with surface O^{2-} dangling bonds significantly increases the emission efficiency of the small-sized sample.

The photoluminescence features were further quantified through the estimation of the absolute emission quantum yield as a function of sample size, as listed in table 1. Under 250 nm excitation (CTB), the small-sized samples (NR and NR1) show a quantum yield of 12.3% and 6.9%, respectively, while the quantum yield values of large-sized samples (NW and NW1) lie below the detection limits of our equipment. Under 274 nm excitation ($^8S_{7/2} \rightarrow {}^6I_J$ transition of Gd^{3+}), the small-sized samples show the quantum yield as almost twofold higher than that of large-sized samples for the same dopant concentration.

Table 1. Absolute emission quantum yields of samples NR, NR1, NW and NW1. ('—' means the quantum yield is below the detection limit of our equipment.)

Excitation wavelength (nm)	QY (%)			
	NR	NW	NR1	NW1
250	12.3	—	6.9	—
274	10.2	5.1	5	3.5

For all samples, the quantum yields of samples with high dopant concentration are relatively high, compared with those samples with low dopant concentration. The above results are in good agreement with the tendency observed in the emission spectra (figure 4).

4. Conclusions

The hexagonal rhabdophane-type $GdPO_4$ hydrate ($GdPO_4 \cdot nH_2O$) was synthesized via a simple hydrothermal process. The pH variation of the precursor solution leads to a significant variation of size of the as-synthesized particles. In the absence of NaOH as a pH modifier (reaction solution pH = 2), nanorods with a width of 50–100 nm and a length of about 1 μm were obtained. However, a significant reduction of size (width: ~10 nm, length: ~50 nm) was observed for the product synthesized in the presence of NaOH (pH = 10). A considerably large variation of the particle size is attributed to the pH of reaction systems and the introduction of alkali metal cations. The controlled size provides the basis for the study of the correlation of size with the photoluminescence properties. Unexpectedly, the emission efficiency of small-sized samples is nearly four times stronger than that of the corresponding large-sized samples. The EDS and XPS measurements revealed the presence of Na^+ in the small-sized samples synthesized in the presence of NaOH. Some of the Na^+ cations probably entered into the linear open tunnels along the c axis in the host. In particular, part of the Na^+ were bonded to the surface O^{2-} dangling bonds, which thus reduces the number of surface defects that usually serve as nonradiative energy transfer centers.

Therefore, a markedly enhanced photoluminescence of small-sized sample should be ascribed to a reduction of surface defect centers due to the bonding of Na^+ with surface O^{2-} dangling bonds. This result is also confirmed by the time-resolved spectra, in which it is observed that the lifetime of Eu^{3+} $^5D_0$ of the small-sized sample (2.86 ms) is much longer than that of the large-sized sample (1.67 ms). Therefore, NaOH plays a key role in the synthesis and properties. On the one hand, the relatively small size can be achieved by adjusting the pH due to the addition of NaOH; on the other hand, the doping of alkali metal Na^+ significantly enhances the photoluminescence efficiency. Our present results imply that the controlled synthesis of rare-earth-doped nanoparticles with a small size, but with relatively strong luminescence has an important significance for their applications in the areas of technologies including optoelectronics, sensing and bioimaging.

Acknowledgments

This work is supported by the National Natural Science Foundation of China (grant nos. 10874180, 10774142, 10834006 and 10774141) and the MOST of China (2006CB601104).

References

[1] Wei Z G, Sun L D, Liao C S, Yin J L, Jiang X C, Yan C H and Lü S Z 2002 *J. Phys. Chem.* B **106** 10610
[2] Qi Z M, Shi C S, Zhang W W, Zhang W P and Hu T D 2002 *Appl. Phys. Lett.* **81** 2857
[3] Bhargava R N 2000 *J. Cryst. Growth* **214/215** 926
[4] Yan C H, Sun L D, Liao C S, Zhang Y X, Lu Y Q, Huang S H and Lü S Z 2003 *Appl. Phys. Lett.* **82** 3511
[5] Bu W B, Chen H R, Hua Z L, Liu Z C, Huang W M, Zhang L X and Shi J L 2004 *Appl. Phys. Lett.* **85** 4307
[6] Pan G H, Song H W, Yu L X, Liu Z X, Bai X, Lei Y Q and Fan L B 2007 *J. Lumin.* **122/123** 882
[7] Di W H, Wang X J, Zhu P F and Chen B J 2007 *J. Solid State Chem.* **180** 467
[8] Ji S L, Yin L L, Liu G D, Zhang L D and Ye C H 2009 *J. Phys. Chem.* C **113** 16439
[9] Di W H, Wang X J, Chan B J, Lu S Z and Ren X G 2006 *Appl. Phys. Lett.* **88** 011907
[10] Su Y G, Li L P and Li G S 2008 *Cryst. Growth Des.* **8** 2678
[11] Williams D K, Bihari B, Tissue B M and McHale J M 1998 *J. Phys. Chem.* B **102** 916
[12] Goldburt E T, Kulkarni B, Bhargava R N, Taylor J and Libera M 1997 *J. Lumin.* **72–74** 190
[13] Wakefield G, Holland E, Dobson P J and Hutchison J L 2001 *Adv. Mater.* **13** 1557
[14] Bühler G and Feldmann C 2006 *Angew. Chem. Int. Edn* **45** 4864
[15] Mai H X, Zhang Y W, Sun L D and Yan C H 2007 *Chem. Mater.* **19** 4514
[16] Antic B, Rogan J, Kremenovic A, Nikolic A S, Vucinic-Vasic M, Bozanic D K, Goya G F and Colomban Ph 2010 *Nanotechnology* **21** 245702
[17] Mass H, Currao A and Calzaferri G 2002 *Angew. Chem. Int. Edn* **41** 2495
[18] Di W H, Willinger M G, Ferreira R A S, Ren X G, Lu S Z and Pinna N 2008 *J. Phys. Chem.* C **112** 18815
[19] Park J C, Moo H K, Kim D K, Byeon S H, Kim B C and Suh K S 2000 *Appl. Phys. Lett.* **77** 2162
[20] Wang G F, Qin W P, Zhang D S, Wang L L, Wei G D, Zhu P F and Kim R J 2008 *J. Phys. Chem.* C **112** 17042
[21] Jia C J, Sun L D, Luo F, Jiang X C, Wei L H and Yan C H 2004 *Appl. Phys. Lett.* **84** 5305
[22] Di W H, Wang X J, Chan B J, Lu S Z and Zhao X X 2005 *J. Phys. Chem.* B **109** 13154
[23] Kömpe K, Borchert H, Storz J, Lobo A, Adam S, Möller T and Hasse M 2003 *Angew. Chem. Int. Edn* **42** 5513
[24] Bai X, Song H W, Pan G H, Liu Z X, Lu S Z, Di W H, Ren X G, Lei Y Q, Dai Q L and Fan L B 2006 *Appl. Phys. Lett.* **88** 143104
[25] Fang Y P, Xu A W, Song R Q, Zhan H X, You L P, Yu J C and Liu H Q 2003 *J. Am. Chem. Soc.* **125** 16025
[26] Luwang M N, Ningthoujam R S, Jagannath, Srivastava S K and Vatsa R K 2010 *J. Am. Chem. Soc.* **132** 2759
[27] Luo Q L, Shen S D, Lu G Z, Xiao X Z, Mao D S and Wang Y Q 2009 *J. Mater. Chem.* **19** 8079
[28] Di W H, Wang X J and Ren X G 2010 *Nanotechnology* **21** 075709
[29] Zhang F and Wong S S 2010 *ACS Nano* **4** 99
[30] Sharma P K, Jilavi M H, Varadan V K and Schmidt H 2002 *J. Phys. Chem. Solids* **63** 171
[31] Zhang Y J and Guan H M 2003 *J. Gryst. Growth* **256** 156
[32] Cho S, Jang J W, Jung S H, Lee B R, Oh E and Lee K H 2009 *Langmuir* **25** 3825
[33] Li C X, Hou Z Y, Zhang C M, Yang P P, Li G G, Xu Z H, Fan Y and Lin J 2009 *Chem. Mater.* **21** 4598
[34] Feng Y, Ma T Y, Liu L and Yuan Z Y 2009 *Chin. Sci.* B **39** 864
[35] Yu S H and Qian Y T 2006 *Self-Organised Nanoscale Materials* (Berlin: Springer)
[36] Chen D Q, Yu Y L, Huang F, Huang P, Yang A P and Wang Y S 2010 *J. Am. Chem. Soc.* **132** 9976
[37] Di W H, Ferreira R A S, Willinger M G, Ren X G and Pinna N 2010 *J. Phys. Chem.* C **114** 6290
[38] Mooney R C L 1950 *Acta Crystallorg.* **3** 337
[39] Tie S L, Su Q and Yu Y Q 1995 *J. Alloys Compounds* **227** 1
[40] Hoefdraad H E 1975 *J. Solid State Chem.* **15** 175